Received 26 August 2023; revised 29 September 2023; accepted 23 October 2023. Date of publication 31 October 2023; date of current version 22 November 2023.

Digital Object Identifier 10.1109/OJCOMS.2023.3328859

Terahertz Communications Between Unstable Transceivers With Pointing Errors Over FTR Fading

ANIL YADAV (Graduate Student Member, IEEE), AND RANJAN K. MALLIK (Fellow, IEEE)

Department of Electrical Engineering, Indian Institute of Technology Delhi, New Delhi 110016, India

CORRESPONDING AUTHOR: A. YADAV (e-mail: anilyadav1597@gmail.com)

ABSTRACT Terahertz (THz) wireless communication has emerged as a promising technology for high-speed, ultra-broadband, and low-latency data transmission. However, the performance of THz systems is significantly affected by various channel and system parameters. Existing literature often models THz transmission links using $\alpha - \mu$ fading with pointing error, which is suitable for optical communication systems or a specific type of THz antennas. A new pointing error model designed for THz antennas has recently been proposed. The fluctuating two-ray (FTR) fading model emerges as a very suitable choice for THz transmission, as it considers the line-of-sight components and their random phase distributions, in addition to multipath and non-linearity of the propagation medium. In this paper, we model a THz transmission link considering FTR short-term fading, channel path loss, and the recently proposed pointing error, with two standard uniform $N \times N$ THz antenna arrays, one mounted at the unstable transmitter and one at the unstable receiver (instability accounts for the dynamic nature of drone-to-drone communication scenarios, particularly, dynamic drones fluctuating in yaw, roll, and pitch directions). Novel exact analytical closed-form expressions for the probability density function, the cumulative distribution function, and moment generating function of the received instantaneous signal-to-noise ratio are derived for the aforementioned system using standard mathematical functions. Next, closed-form expressions for performance metrics, namely, the outage probability, the average bit error rate, and the average channel capacity, are derived. Furthermore, the nth moment of the received instantaneous signal-to-noise ratio and diversity order of the system are derived. The effects of various channel and system parameters on the system performance are studied, and the accuracy of the derived analytical expressions is confirmed by simulation results.

INDEX TERMS Antenna arrays, fluctuating two-ray (FTR) fading, pointing errors, terahertz (THz) communication.

I. INTRODUCTION

THE UTILIZATION of terahertz (THz) technology holds great promise for future wireless communication systems, enabling high-speed data transmission with ultra-high bandwidth and minimal latency [1], [2], [3], [4], [5], [6], [7]. In response to the exponential growth of data traffic in wireless communications, the THz frequency range is being actively considered as a potential solution to support ultra-broadband requirements in upcoming generations [4]. To meet the escalating demand for bandwidth and data rates, the unlicensed THz spectrum is being explored as a valuable resource [5]. Particularly, in wireless backhaul and fronthaul technology, the THz spectrum ($0.1-10$ THz) offers significant potential for transmitting data with remarkable bandwidth capacity [6]. Touchless mobile technologies, online gaming, augmented reality (AR), virtual reality (VR), and similar applications necessitate data rates of up to 10 Tbps [7]. THz technology holds the potential to deliver data rates of up to 1 Tbps, offering a promising solution to meet these requirements.

Modeling multipath fading for THz wireless transmissions is of utmost importance to researchers. Researchers demonstrated that the fluctuating two-ray (FTR) model fits THz multipath fading more accurately in contrast to the traditional

Rician and Nakagami-m distributions [8], [9], [10]. The FTR fading model has been demonstrated to accurately match field measurements across a range of propagation scenarios [11] and offers a more accurate fit to the field measurements compared to other traditional fading models [12], for example, the 28 GHz field measurements recently reported in [13]. Highly directional THz antennas experience misalignment between the transmitter and receiver antennas, a phenomenon commonly referred to as pointing error. This misalignment can have adverse effects on the received signal strength and can lead to a degradation in link performance. The authors in [14] derive the outage probability and ergodic capacity by combining the effects of FTR short-term fading, pointing error, and hardware defects for reconfigurable intelligent surface (RIS)-aided THz systems. In [15], an analytical methodology for quantifying and evaluating the combined effect of misaligned fading and hardware imperfections in the presence of multipath fading is examined by the authors. In [16], the authors analyze the system performances in terms of the outage probability (OP), the average bit error rate (BER), and the ergodic capacity for single antenna reception and multi-antenna reception with maximal ratio combining by combining the effect of FTR short-term fading and pointing error for THz system. The pointing error used in most of the studies for the THz band [14], [15], [16] is valid only for a special type of antennas. In [17], the authors propose a new pointing error model for THz communication using two $N \times N$ conventional antenna arrays, one positioned at the unstable (also termed as fluctuating) transmitter and one at the unstable receiver (the instability at the transmitter and receiver accounts for the dynamic nature of drone-to-drone communication scenarios, particularly, dynamic drones fluctuating in yaw, roll, and pitch directions). In [18], the authors examine the combined impact of the newly proposed pointing errors for the THz band and $\alpha - \mu$ fading on the system performance. It should be noted that the $\alpha - \mu$ fading model only takes the effect of the multipath and the propagation medium's non-linearity into account. The random phase distributions of the line-of-sight components, which are not taken into account in the $\alpha - \mu$ fading model, are taken into account in the FTR fading model (this model also considers the multipath and the non-linearity of the propagation medium) [12]. To the best of our knowledge, there is no open literature that discusses the combined effect of the newly proposed pointing errors over FTR fading for THz wireless transmission. In this paper, we examine the combined effect of FTR short-term fading and the newly derived pointing error for the THz band, considering two standard uniform $N \times N$ antenna arrays, one mounted at the unstable transmitter and one at the unstable receiver. The following are the main contributions:

- We present novel closed-form expressions for the probability density function (PDF), the cumulative distribution function (CDF), and the moment generating function (MGF) of the instantaneous received signal-to-noise ratio (SNR) in a THz transmission system taking into account the effects of FTR short-term fading, channel path loss, and the recently proposed pointing error. To gain a deeper understanding of this analysis, we proceed to derive the analytical expressions for the nth moment of the received instantaneous SNR.
- We derive an exact analytical closed-form expression for the OP in terms of the single-variate Fox's H-function. We demonstrate how the system performance, as quantified by the OP, is influenced by factors such as the transmission distance, the size of transmit and receive antenna arrays, the angular instability, and the FTR fading parameters.
- We derive an exact analytical closed-form expression for the average BER in terms of the single-variate Fox's H-function. We determine the diversity order in terms of the system parameters. We demonstrate the impact of the transmission distance, the size of transmit and receive antenna arrays, the angular instability, and the FTR fading parameters on the system performance in terms of the average BER.
- Next, we derive an exact analytical closed-form expression of the average channel capacity in terms of the single-variate Fox's H function, and demonstrate the impact of the transmission distance, the size of transmit and receive antenna arrays, the angular instability, and the FTR fading parameters on the system performance in terms of the average channel capacity.
- We verify the accuracy of the derived analytical expressions by employing the Monte Carlo simulations (averaged over 10^7 channel realizations).

A. RELATED WORK

The newly introduced FTR model has been extensively studied for mmWave wireless communication [19], [20], [21], [22]. In [19], the study of ergodic capacity is conducted for FTR fading channels under various power adaptation techniques. In [20], the authors investigated the physical layer secrecy performance over the FTR fading channel. In [21], the authors examined the performance of a dual-hop system that combines free-space optics (FSO) and millimeter-wave (mmWave) technologies and modeled the channels as gamma-gamma and FTR distributions, respectively. In [22], the authors formulated noval exact analytical expressions for multiple statistical metrics concerning the product of N independent FTR random variables. In [23], the authors conducted the two THz signal measurement experiments in different scenarios to prove the validity of FTR fading to be considered as a small-scale amplitude fading of THz signals. The literature utilizes the pointing error proposed in [24] (which is appropriate for optical communication or a special case of THz systems) to model the THz transmission links [14], [15], [16], [23], [25], [26], [27], [28], [29]. However, a new pointing error is derived in [17] for standard uniform $N \times N$ antenna arrays, one

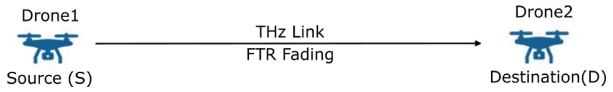

FIGURE 1. THz Communication System Model.

mounted at the unstable transmitter and one at the unstable receiver with the consideration of similar vibrations in the yaw and pitch directions, and is generalized in [30] for different antenna patterns at the transmitter and receiver, and the dissimilar vibrations in the yaw and pitch directions for THz communications. It is shown in [17] that the previously used pointing error for THz communications in the literature in [14], [15], [16], [23], [25], [26], [27], [28], [29] which is suitable for optical communication systems and a special case of THz systems, cannot be directly used for the typical THz communication system. Recently the newly derived pointing error is used for studying and designing high-directional THz systems [18]. In the light of this research, we design a THz transmission link considering two standard uniform $N \times N$ antenna arrays, one mounted at the unstable transmitter and one at the unstable receiver, with the consideration of the path loss, the FTR short-term fading (which is a valid model for small-scale fading of THz links), and the recently proposed pointing error, and reanalyze the system performances.

B. NOTATIONS AND ORGANIZATION

The key notations are presented in Table 1. The paper is structured as follows. Section II is dedicated to the discussion of the system model. In Section III, we derive the statistical characteristics of the received SNR, including the PDF, CDF, MGF, nth moment, and amount of fading (AoF). In Section IV, we analyze the system performance by deriving closed-form expressions for the average BER and the average channel capacity. Additionally, within this section, we also determine the diversity order to gain a deeper understanding of the system's performance. In Section V, we present the numerical results of the analyzed system. Finally, in Section VI, we draw conclusions based on our findings.

II. SYSTEM MODEL

In this section, we present the considered system model and provide a brief introduction to the key factors influencing the design of the THz wireless transmission link. A THz transmission link is considered as shown in Fig. 1, where we consider two drones drone-1 and drone-2 as source (S) and destination (D), respectively, which are communicating at THz frequency range.

The factors that can affect a THz transmission link are path loss, molecular absorption, small-scale fading, pointing errors, and hardware impairments. We assume negligible hardware impairments in this study. In designing the THz transmission link, we take into account the combined impact of path loss, molecular absorption, short-term fading, and pointing errors.

TABLE 1. List of symbols.

Symbol	Parameter
m, K, Δ	Fading parameters
ϕ, w_z, σ_θ	Pointing error parameter
h	Channel coefficient
ν	Frequency of operation
W	Bandwidth
T	Absolute temperature
p	Atmospheric pressure
ψ	Relative humidity
$N \times N$	Size of THz antenna array
h_f	Small scale fading
h_p	Pointing error coefficient
$f(z)$	Probability density function
$M(z)$	Moment-generating function
$F(z)$	Cumulative distribution function
γ	Signal to noise ratio
P_b	Average SER
$G_{p,q}^{m,n}(.)$	Meijer G-function
$H_{p,q}^{m,n}(.)$	Fox's H-function
${}_2F_1(\cdot,\cdot;\cdot;\cdot)$	Gauss hypergeometric function
$\Gamma(n)$	$\int_0^\infty x^{n-1}e^{-x}dx$
$(\rho)_q$	Pochhammer's symbol

Taking into account the combined impact of path loss, molecular absorption, small-scale fading, and pointing errors and by considering the effect of all the antenna elements of transmit and receive antenna arrays, the expression for the complex channel coefficient of the considered transmission link is given by [31]

$$h = h_l h_f h_p S_0 \tag{1}$$

where h_l is the deterministic path loss ($h_l > 0$), h_f is the complex small-scale fading coefficient, h_p is the pointing error coefficient ($h_p > 0$), and S_0 is the maximum antenna pattern gain ($S_0 > 0$). Here is a brief introduction to the key factors considered in link designing.

A. MOLECULAR ABSORPTION AND PATH LOSS

Molecular absorption and path loss are deterministic in nature and the overall deterministic path loss $h_l = h_{lf} h_{lm}$, where according to Friis transmission equation $h_{lf} = (\frac{\lambda}{4\pi d})^2$ denotes the free space path loss, $h_{lm} = \exp(-\frac{K(\nu)d}{2})$ represents the molecular absorption loss, and λ and d denote the wavelength and transmission distance (link length), respectively. The quantity $K(\nu)$ is the absorption

coefficient, which is a function of the frequency, temperature, atmospheric pressure, and relative humidity, and is given in [32].

B. SMALL-SCALE FADING

To model small-scale fading, the FTR fading model is used. The FTR fading model is designed to characterize wireless communication scenarios where there are two dominant signal components and a diffuse component, described as

- First dominant/specular component (typically direct path; line-of-sight (LOS) component): This is the primary signal component where the signal travels directly from the transmitter to the receiver without any reflection. It is usually the shortest and most significant contributor to the received signal.
- Second dominant/specular component (typically dominant reflected component): In this model, the reflected component typically represents a signal that reflects off a nearby surface before reaching the receiver. The reflecting surface can be the ground, a building, or any other obstacle.
- Nonspecular component: A nonspecular component is a group of two or more terms representing more than one multipath waves arriving at the receiver.
- Diffuse component: A diffuse component is a nonspecular component with numerous individual waves, each carrying power that is negligible compared to the total average power of the diffuse component.

The term "fluctuating" in this model indicates that the signal experiences fluctuations in its strength or quality. These fluctuations occur due to various factors, such as multipath fading, non-linearity of the propagation medium, environmental changes, and channel dynamics.

The FTR fading model has applications in various wireless communication systems, including outdoor scenarios where both line-of-sight and reflected paths are relevant.

In accordance with the FTR fading model, the complex baseband representation of the response of the wireless channel can be formulated as

$$A_r = \sqrt{\upsilon}A_1 \exp(\imath\varphi_1) + \sqrt{\upsilon}A_2 \exp(\imath\varphi_2) + T_1 + \imath T_2, \quad (2)$$

where υ represents a gamma-distributed random variable with unit mean, A_1 and A_2 are constant amplitudes having specular components modulated by a Nakagami-m random variable, $\imath = \sqrt{-1}$, and ϕ_1 and ϕ_2 are uniformly distributed random phases with $\phi_1,\ \phi_2 \sim U[0, 2\pi)$. Furthermore, $T_1 + \imath T_2$ represents the diffuse component, which can be characterized as a complex Gaussian random variable with each of T_1 and T_2 following a normal distribution $N(0, \sigma^2)$. The FTR fading model can be succinctly represented by introducing the parameters K and Δ, which are expressed, respectively, as

$$K = \frac{A_1^2 + A_2^2}{2\sigma^2}, \quad (3)$$

$$\Delta = \frac{2A_1A_2}{A_1^2 + A_2^2}. \quad (4)$$

The parameter K is the ratio of the average power of the dominant components to that of the remaining diffused components and Δ describes the relationship between the powers of the two dominant components and varies from 0 to 1. The magnitudes of the two dominant waves are equivalent when $\Delta = 1$. When $\Delta = 0$, the FTR fading model is reduced to a single-component Rician shadowed fading model. The PDF of the magnitude-square of the complex small-scale fading coefficient h_f is given by [33]

$$f_{|h_f|^2}(x) = \frac{m^m}{\Gamma(m)} \sum_{r=0}^{\infty} \frac{K^r d_r x^r}{(\Gamma(r+1))^2} \exp\left(-\frac{x}{2\sigma^2}\right) \quad x > 0, \quad (5)$$

where m is the fading severity index, and the coefficient d_r is expressed as

$$\begin{aligned} d_r \triangleq & \sum_{k=0}^{r} \binom{r}{k} \sum_{i=0}^{k} \binom{k}{i} \Gamma(r+m+2i-k) \\ & \times (m+k)^{-(r+m+2i-k)} \\ & \times K^{2i-k} \left(\frac{\Delta}{2}\right)^{2i} (-1)^{2i-k} R_{r+m}^{k-2i}\left(\left[\frac{K\Delta}{m+k}\right]^2\right). \end{aligned} \quad (6)$$

The function $R_\zeta^\eta(w)$ in (6) is defined as

$$R_\zeta^\eta(w) \triangleq \begin{cases} \left(\frac{\eta-\zeta}{2}\right)_\zeta \left(\frac{\eta-\zeta+1}{2}\right)_\zeta \frac{w^\zeta}{\zeta!} \\ \times {}_2F_1\left(\frac{\eta-\zeta}{2}, \frac{\eta-\zeta+1}{2}; 1-\zeta; w\right) \\ \text{if } \zeta \in \mathbb{N} \\ \frac{{}_2F_1\left(\frac{\eta-\zeta}{2}, \frac{\eta-\zeta+1}{2}; 1-\zeta; w\right)}{\Gamma(1-\zeta)} \\ \text{otherwise,} \end{cases} \quad (7)$$

where $(\rho)_q = \Gamma(\rho+q)/\Gamma(\rho)$ and $\mathbb{N}$ is the set of natural numbers.

C. POINTING ERROR

The random movement of transmit and receive drones due to wind or hovering fluctuations in yaw, roll, and pitch directions leads to pointing errors. As shown in Fig. 2, orientation deviations in the directions of yaw and pitch are equivalent to the orientation deviations in $x-z$ and $y-z$ planes, respectively. By considering the effect of all antenna elements of transmit and receive antenna arrays at once, the uniform standard $N \times N$ transmit and receive antenna arrays can be treated as a single antenna with a gain equivalent to the array radiation gain (gain of single antenna multiplied by the array factor/gain) [34]. The overall array radiation gain of the transmit and receive standard uniform $N \times N$ antenna array can be written as $S_0(N)\sqrt{S_t(\theta_{tx}, \theta_{ty})S_r(\theta_{rx}, \theta_{ry})}$, where the coefficient $S_0(N)$ and the array radiation gain in the direction of θ_{qx} and θ_{qy} are given, respectively, as [34]

$$S_0(N) = 4\pi \left(\int_0^{\pi} \int_0^{2\pi} S_q(\theta_{qx}, \theta_{qy}) sin(\theta_{qx}) d\theta_{qx} d\theta_{qy} \right)^{-1}$$

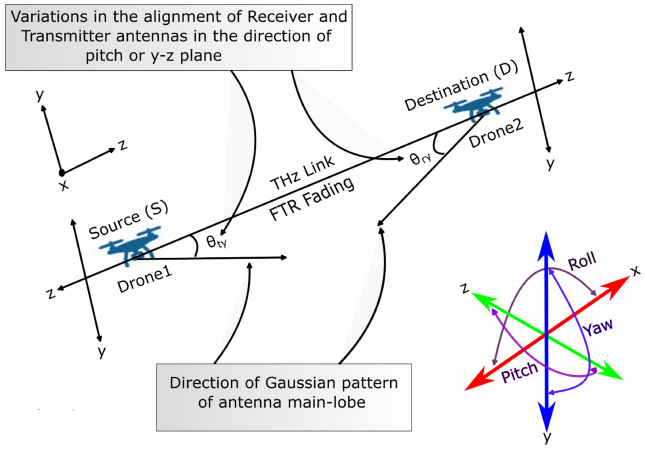

FIGURE 2. Orientation fluctuation causing pointing error.

and

$$S_q(\theta_{qx},\theta_{qy}) = S_0(N) \times \left(\frac{\sin\left(\frac{N(kd_x\sin(\theta_{qx})\cos(\theta_{ty}))}{2}\right)}{N^2\sin\left(\frac{kd_x\sin(\theta_{qx})\cos(\theta_{qy})+\beta_x}{2}\right)}\frac{\sin\left(\frac{N(kd_y\sin(\theta_{qx})\sin(\theta_{qy}))}{2}\right)}{\sin\left(\frac{kd_y\sin(\theta_{qx})\sin(\theta_{qy})}{2}\right)}\right)^2,$$

where $q \in \{t, r\}$ determines the transmitter and receiver nodes. Therefore, the uniform standard $N \times N$ antenna array can be considered as a single antenna with a gain equivalent to the array radiation gain. Consequently, the channel coefficient can be treated as a one-dimensional scalar rather than an $N \times N$ matrix. By taking into account the equal intensity of vibration experienced by both the transmitter and receiver in the yaw and pitch directions, and considering minimal orientation deviations in the roll direction, the PDF of the recently proposed pointing error coefficient h_p, which is a function of the number of antenna elements is expressed as [17]

$$f_{h_p}(y) = -\phi^2 y^{\phi-1}\ln y \quad 0 < y < 1, \tag{8}$$

where $\phi = w_z^2/\sigma_\theta^2$, with w_z denoting the antenna beamwidth and σ_θ^2 denoting the variance of the antenna orientation fluctuations. For a uniform standard $N \times N$ antenna array, w_z and the maximum antenna pattern gain S_0 in (1) can be well approximated as $1.061/N$ and πN^2, respectively [17]. Please note that this expression of the PDF of the pointing error is valid for a point-to-point communication link between two identical standard uniform $N \times N$ antenna arrays (one mounted at the unstable transmitter and one at the unstable receiver). For more in-depth information about the PDF of the newly introduced pointing error coefficient, please refer to [17].

The *instantaneous received SNR*, denoted by γ, is expressed as $\gamma = \gamma_0 S_0^2 h_l^2 |h_f|^2 h_p^2$, where the term γ_0 is defined as $\gamma_0 \triangleq P_t/(N_0 W)$, with P_t denoting the transmit power, W denoting the width of the frequency band, and $N_0 = K_b T$ denoting the thermal noise power spectral density. where K_b represent the Boltzmann's constant.

III. STATISTICS OF RECEIVED SNR

In this section, exact closed-form expressions for the PDF, the CDF, and the MGF of the received SNR are derived in terms of the single variate Fox's H function. These results are crucial for analyzing the system's performance and deriving analytical expressions for the BER and average channel capacity. we also calculate the nth moment of the received SNR, which serves as a basis for analyzing other statistical parameters like average SNR and AoF.

Theorem 1: Analytical closed-form expressions for the PDF, the CDF, and the MGF of the instantaneous received SNR γ are given by

$$f_\gamma(z) = \frac{\phi^2 m^m}{4\delta\Gamma(m)}\sum_{r=0}^{\infty}\frac{K^r d_r z^r}{(2\sigma^2)^r\Gamma^2(r+1)\left(S_0^2\gamma_0 h_l^2\right)^r} \times H_{2,3}^{3,0}\left[\frac{z}{\delta}\middle|\begin{matrix}(a,1),(a,1)\\(0,1),(a-1,1),(a-1,1)\end{matrix}\right], \tag{9}$$

$$F_\gamma(z) = \frac{\phi^2 m^m}{4\delta\Gamma(m)}\sum_{r=0}^{\infty}\frac{K^r d_r z^{r+1}}{(2\sigma^2)^r\Gamma^2(r+1)\left(S_0^2\gamma_0 h_l^2\right)^r} \times H_{3,4}^{3,1}\left[\frac{z}{\delta}\middle|\begin{matrix}(-r,1),(a,1),(a,1)\\(0,1),(a+1,1),(a+1,1),(-(r+1),1)\end{matrix}\right], \tag{10}$$

and

$$M_\gamma(\omega) = \frac{\phi^2 m^m}{4\delta\Gamma(m)}\sum_{r=0}^{\infty}\frac{K^r d_r}{(2\sigma^2)^r\Gamma^2(r+1)\left(S_0^2\gamma_0 h_l^2\right)^r} \frac{1}{(-\jmath\omega)^{r+1}} \times H_{3,3}^{3,1}\left[\frac{-1}{\jmath\omega\delta}\middle|\begin{matrix}(-r,1),(a,1),(a,1)\\(0,1),(a-1,1),(a-1,1)\end{matrix}\right] \tag{11}$$

respectively, where $a = (\phi/2) - r$ and $\delta = 2\sigma^2 S_0^2\gamma_0 h_l^2$.

Proof: The proof is given in Appendix A. ■

Lemma 1: The nth moment of the instantaneous received SNR is given as

$$\bar{\gamma}^{(n)} = \frac{\phi^2 m^m}{4\delta\Gamma(m)}\sum_{r=0}^{\infty}\frac{K^r d_r}{(2\sigma^2)^r\Gamma^2(r+1)\left(S_0^2\gamma_0 h_l^2\right)^r} \times H_{3,4}^{3,1}\left[\frac{1}{\delta}\middle|\begin{matrix}(-(r+n),1),(a,1),(a,1)\\(0,1),(a-1,1),(a-1,1),(-(n+r+1),1)\end{matrix}\right]. \tag{12}$$

The expression derived for the nth moment of the instantaneous received SNR in Lemma 1 can be applied to compute the average SNR by setting $n = 1$ in (12). Moreover, a closed-form expression for the 2^{nd} order AoF equals

$$AoF = \frac{\bar{\gamma}^{(2)}}{\left(\bar{\gamma}^{(1)}\right)^2} - 1. \tag{13}$$

Proof: The proof is given in Appendix B. ■

IV. PERFORMANCE ANALYSIS

In this section, we derive analytical closed-form expressions of performance metrics in terms of the OP, the average BER, the average channel capacity, and the ergodic mutual information. Moreover, to gain a deeper understanding of the system's performance, we compute the diversity order of the system under consideration.

A. OUTAGE PROBABILITY

An accurate formulation for the OP is expressed as $P_{out} = F_\gamma(\gamma_{th})$, where $F_\gamma(z)$ is provided by equation (10), and γ_{th} represents the threshold SNR value.

B. AVERAGE BIT ERROR RATE

For the AWGN channel, the average BER expression for various binary modulation techniques is given by [33, eq. (15)]

$$P_b = \frac{{c_1}^{c_2}}{2\Gamma(c_2)} \int_0^\infty z^{c_2-1} e^{-c_1 z} F_\gamma(z)\, dz, \tag{14}$$

where $(c_1, c_2) = (1, 0.5)$ for binary phase-shift keying (BPSK), $(c_1, c_2) = (0.5, 0.5)$ for coherent binary frequency-shift keying (BFSK), and $(c_1, c_2) = (1, 1)$ for differential BPSK. Substituting (10) in (14) and interchanging the order of integration and summation, we get

$$\begin{aligned} P_b = {} & \frac{\phi^2 m^m {c_1}^{c_2}}{8\delta\Gamma(m)\Gamma(c_2)} \sum_{r=0}^{\infty} \frac{K^r d_r}{\left(2\sigma^2\right)^{(r)} \Gamma^2(r+1)\left(S_0^2\gamma_0 h_l^2\right)^r} \\ & \times \int_0^\infty z^{r+b} H_{0,1}^{1,0}\left[c_1 z \middle| \begin{matrix} () \\ (0,1) \end{matrix}\right] \\ & \times H_{3,4}^{3,1}\left[\frac{z}{\delta}\middle| \begin{matrix} (-r,1),(a,1),(a,1) \\ (0,1),(a+1,1),(a+1,1),(-(r+1),1) \end{matrix}\right] dz. \end{aligned} \tag{15}$$

Next, making use of [35, Th. 2.9], (15) is expressed in the form of Fox's H-functions as

$$\begin{aligned} P_b = {} & \frac{\phi^2 m^m}{8\delta\Gamma(m)\Gamma(c_2)} \sum_{r=0}^{\infty} \frac{K^r d_r}{\left(2\sigma^2\right)^r \Gamma^2(r+1)\left(S_0^2\gamma_0 h_l^2\right)^r} \\ & \times H_{4,4}^{3,2}\left[\frac{1}{c_1\delta}\middle| \begin{matrix} (-r,1),(-r-b,1),(a,1),(a,1) \\ (0,1),(a+1,1),(a+1,1),(-(r+1),1) \end{matrix}\right]. \end{aligned} \tag{16}$$

C. AVERAGE CHANNEL CAPACITY

The average channel capacity is given by

$$\begin{aligned} C &= \frac{1}{\ln(2)} \int_0^\infty \ln(1+z) f_\gamma(z)\, dz \\ &= \frac{1}{\ln(2)} \int_0^\infty \frac{\left(1 - F_\gamma(z)\right)}{(1+z)} dz. \end{aligned} \tag{17}$$

Plugging (10) into (17) and representing the Fox's H-function in terms of the Mellin-Barnes type integral, we get

$$\begin{aligned} C = {} & \frac{1}{\ln 2} \int_0^\infty \frac{1}{(1+z)} \frac{\phi^2 m^m}{4\delta\Gamma(m)} \sum_{r=0}^{\infty} \frac{K^r d_r z^{r+1}}{(\delta)^r \Gamma^2(r+1)} \frac{1}{(2\pi\jmath)} \\ & \times \oint_{\mathcal{L}} \frac{\Gamma(s)\Gamma^2\left(\frac{\phi}{2} - r - 1 + s\right)}{\Gamma^2\left(\frac{\phi}{2} - r + s\right)} \underbrace{\int_z^\infty x^{r-s} dx}_{I_1} \left(\frac{1}{\delta}\right)^{-s} ds, \end{aligned} \tag{18}$$

where $\jmath = \sqrt{-1}$ and $\mathcal{L}$ is the infinite contour defined in [35, eq. (1.1.6)]. Representing I_1 in terms of the fraction of gamma functions by using identities [36, eq. (4.293.3)] and [37, eq. (1.1.8)], (18) is expressed as

$$\begin{aligned} C = {} & \frac{1}{\ln 2} \int_0^\infty \underbrace{\frac{1}{(1+z)}}_{T_1} \frac{\phi^2 m^m}{4\delta\Gamma(m)} \sum_{r=0}^{\infty} \frac{K^r d_r z^{r+1}}{(\delta)^r \Gamma^2(r+1)} \frac{1}{(2\pi\jmath)} \\ & \times \underbrace{\oint_{\mathcal{L}} \frac{\Gamma(s)\Gamma^2\left(\frac{\phi}{2} - r - 1 + s\right)\Gamma(s-r-1)}{\Gamma^2\left(\frac{\phi}{2} - r + s\right)\Gamma(s-r)} \left(\frac{1}{\delta}\right)^{-s} ds}_{T_2}. \end{aligned} \tag{19}$$

By utilizing the identities [37, eq. (2.9.5)] and [37, eqs. (1.1.1) and (1.1.2)], T_1 and T_2 can be written in terms of the Fox's H-function as

$$T_1 = H_{1,1}^{1,1}\left[z\middle| \begin{matrix} (a,1) \\ (0,1) \end{matrix}\right], \tag{20}$$

$$T_2 = H_{3,4}^{4,0}\left[\frac{z}{\delta}\middle| \begin{matrix} (a,1),(a,1),(-r,1) \\ (0,1),(a-1,1),(a-1,1),(-(r+1),1) \end{matrix}\right]. \tag{21}$$

Substituting T_1 and T_2 in (19) and changing the order of integration and summation, (19) is rewritten as

$$\begin{aligned} C = {} & \frac{1}{\ln(2)} \frac{\phi^2 m^m}{4\delta\Gamma(m)} \sum_{r=0}^{\infty} \frac{K^r d_r}{\left(2\sigma^2\right)^r \Gamma^2(r+1)\left(S_0^2\gamma_0 h_l^2\right)^r} \\ & \times \int_0^\infty z^{r+1} H_{1,1}^{1,1}\left[z\middle| \begin{matrix} (a,1) \\ (0,1) \end{matrix}\right] \\ & \times H_{3,4}^{4,0}\left[\frac{z}{\delta}\middle| \begin{matrix} (a,1),(a,1),(-r,1) \\ (0,1),(a-1,1),(a-1,1),(-(r+1),1) \end{matrix}\right] dz. \end{aligned} \tag{22}$$

Finally using [35, eq. (2.8.4)] to solve the inner integration of (22), a closed-form expression for the average channel capacity is obtained as

$$\begin{aligned} C = {} & \frac{1}{\ln(2)} \frac{\phi^2 m^m}{4\delta\Gamma(m)} \sum_{r=0}^{\infty} \frac{K^r d_r}{\left(2\sigma^2\right)^r \Gamma^2(r+1)\left(S_0^2\gamma_0 h_l^2\right)^r} \\ & \times H_{4,5}^{5,1}\left[\frac{1}{\delta}\middle| \begin{matrix} (-r-1,1),(a,1),(a,1),(-r,1) \\ (0,1),(a-1,1),(a-1,1),(-r-1,1),(-r-1,1) \end{matrix}\right]. \end{aligned} \tag{23}$$

Theorem 2: The ergodic mutual information of the $M-QAM$ constellation is derived as

$$\bar{C}(\gamma) = \log_2(M) - \log_2(M) \sum_{\tau=1}^{k_M} \frac{\phi^2 m^m \epsilon_\tau}{4\delta\Gamma(m)}$$

$$\times \sum_{r=0}^{\infty} \frac{K^r d_r}{\left(2\sigma^2\right)^r \Gamma^2(r+1)\left(S_0^2 \gamma_0 h_l^2\right)^r} \times \frac{1}{(V_\tau)^{r+1}} H_{3,3}^{3,1}\left[\frac{1}{\delta V_\tau}\middle| \begin{matrix}(-r,1)(a,1),(a,1)\\(0,1),(a-1,1),(a-1,1)\end{matrix}\right], \tag{24}$$

Proof: The proof is given in Appendix C. ■

D. DIVERSITY ORDER

The diversity order in terms of the average BER is defined as

$$d^{BER} \triangleq -\lim_{\gamma_0 \to \infty} \frac{\log(P_b(\gamma_0))}{\log(\gamma_0)}, \tag{25}$$

where γ_0 represents the transmit power to noise power ratio. In order to calculate the diversity order of the system we express the average BER at high SNR as [35, Th. 1.11]

$$P_b^{\infty} = \frac{\phi^2 m^m}{8\delta\Gamma(m)\Gamma(c_2)} \sum_{r=0}^{\infty} \frac{K^r d_r}{\left(2\sigma^2\right)^r \Gamma^2(r+1)\left(S_0^2\gamma_0 h_l^2\right)^r} \times \sum_{u=1}^{3} \frac{1}{\beta_u} \frac{\prod_{v=1}^{3} \Gamma\left(b_v - b_u \frac{\beta_u}{\beta_v}\right) \prod_{v=1}^{2} \Gamma\left(1 - a_v + b_u \frac{\alpha_v}{\beta_u}\right)}{\prod_{v=3}^{4} \Gamma\left(a_v - b_u \frac{\alpha_v}{\beta_u}\right)\left(1 - b_4 + b_4 \frac{\beta_4}{\beta_u}\right)}, \tag{26}$$

where the coefficients (a_1, a_2, a_3, a_4) and (b_1, b_2, b_3, b_4) are $(-r, -r-b, a, a)$ and $(0, a+1, a+1, -r-1)$ respectively and $(\alpha_1 = \alpha_2 = \alpha_3 = \alpha_4 = \beta_1 = \beta_2 = \beta_3 = \beta_4 = 1)$. By utilizing the asymptotic expressions of the average BER given by (26) and analyzing the dominant terms of the average BER at high SNR, we can readily obtain the system's diversity order as $\frac{\phi+1}{2}$. The expression of diversity order relies on the pointing error parameter ϕ, and this parameter is influenced by both the antenna beamwidth and the degree of antenna orientation fluctuations. It is evident that the diversity order is directly proportional to the square of the antenna beamwidth, denoted as w_z^2, and inversely proportional to the square of the antenna orientation deviation, represented by σ_θ^2. This observation suggests that by adequately adjusting the antenna beamwidth, we can mitigate the influence of antenna orientation deviation. Furthermore, it is possible to enhance the diversity order to some extent by improving the antenna beamwidth while keeping the antenna orientation deviation constant.

V. NUMERICAL RESULTS

In this section, we outline the values of constants and coefficients employed in the MATLAB simulations and analytical results generation. We employ Monte Carlo simulations (averaged over 10^7 channel realizations) to demonstrate the validity of the derived analytical expressions. Additionally, we investigate the impact of the transmission distance, the size of transmit and receive antenna arrays, the angular instability, and the FTR fading parameters on the OP, the average BER, and the average channel capacity.

For our study, we consider two uniform standard $N \times N$ antenna arrays, one mounted at the unstable transmitter and one at the unstable receiver. To ensure computational tractability, the infinite summation is truncated at $r = 27$. The generated plots depict the results for BPSK modulation, where we assign coefficients of $c_1 = 1$ and $c_2 = 0.5$. Other simulation parameters are presented in Table 2. Fig. 3 illustrates the impact of the transmission distance and the antenna array size on the OP. Fig. 3 illustrates that in order to enhance the outage performance of the system, one can either decrease the transmission distance or increase the size of the antenna array.

Fig. 4 showcases the effect of the pointing error on the OP. The OP experiences notable fluctuations as the transceiver instability is altered within the range of 0.8° to 1.2°.

The influence of fading parameters m, K, and Δ (assuming $\sigma^2 = 1$) on the OP is demonstrated in Figs. 5, 6, and 7,

TABLE 2. List of simulation parameters.

Parameter	Value
N	20, 25
ν	120 GHz
W	10^9 Hz
d	250 m, 450 m, 500 m
T	300 K
p	101325 Pa
K_b	1.380649×10^{-23} $m^2kgs^{-2}K^{-1}$
ψ	50%
r	27
σ_θ	$0.8° - 1.8°$
m	0.2−5
K	5−15
Δ	0.2−0.9
σ^2	1

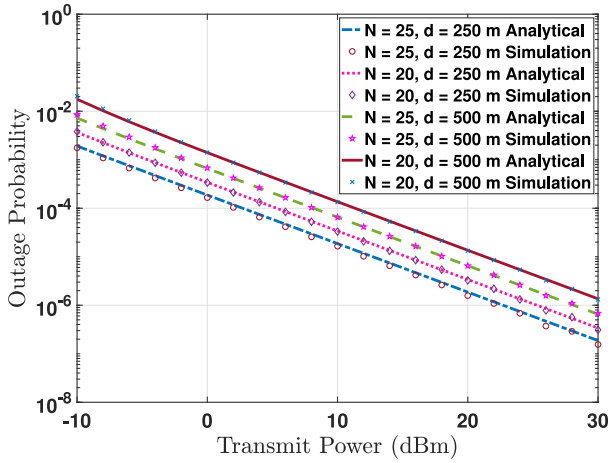

FIGURE 3. Outage probability versus transmit power for varying d and N with parameters $m = 2.3$, $K = 10$, $\sigma^2 = 1$, $\Delta = 0.9$ and $\sigma_\theta = 0.8°$.

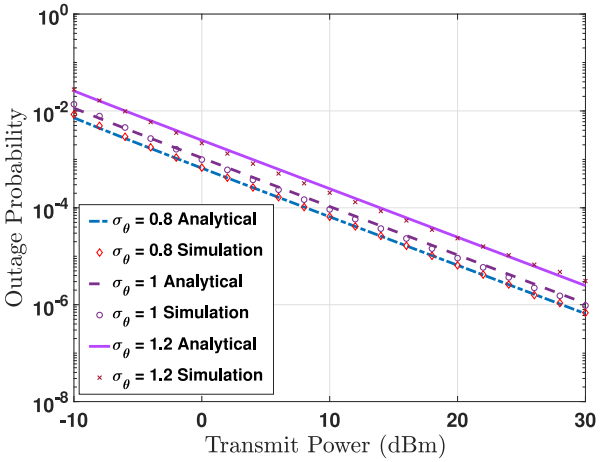

FIGURE 4. Outege probability versus transmit power for varying σ_θ (in degrees) with $d = 450\,\text{m}$, $N = 25$, $m = 2.3$, $K = 10$, $\sigma^2 = 1$, and $\Delta = 0.9$.

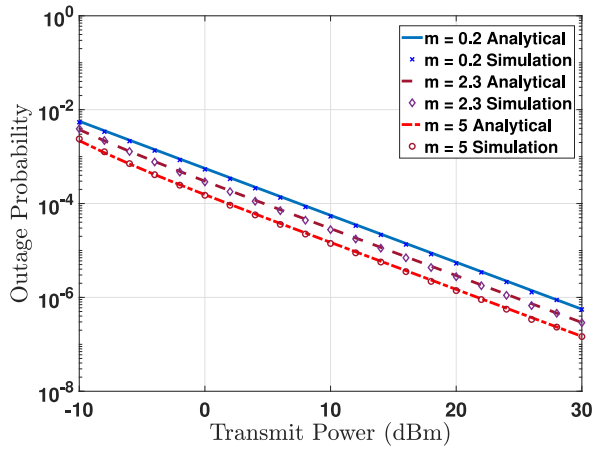

FIGURE 5. Outage probability versus transmit power for varying m with $d = 450\,\text{m}$, $N = 25$, $\sigma_\theta = 0.8°$, $K = 10$, $\sigma^2 = 1$, and $\Delta = 0.5$.

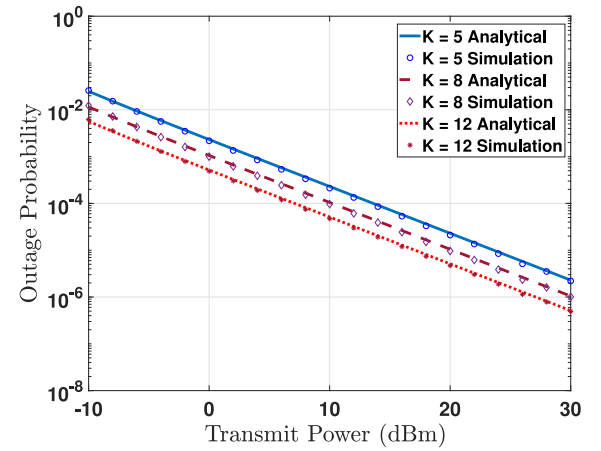

FIGURE 6. Outage probability versus transmit power for varying k with $d = 450\,\text{m}$, $N = 25$, $m = 1$, $\sigma_\theta = 0.8°$, $\sigma^2 = 1$, and $\Delta = 0.5$.

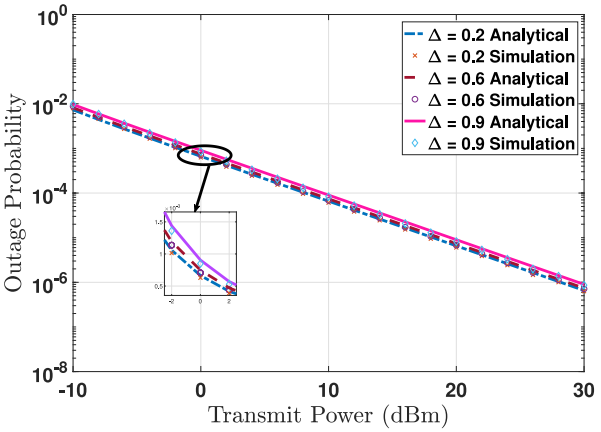

FIGURE 7. Outage probability versus transmit power for varying Δ with $d = 450\,\text{m}$, $N = 25$, $m = 1$, $\sigma_\theta = 0.8°$, $K = 10$, and $\sigma^2 = 1$.

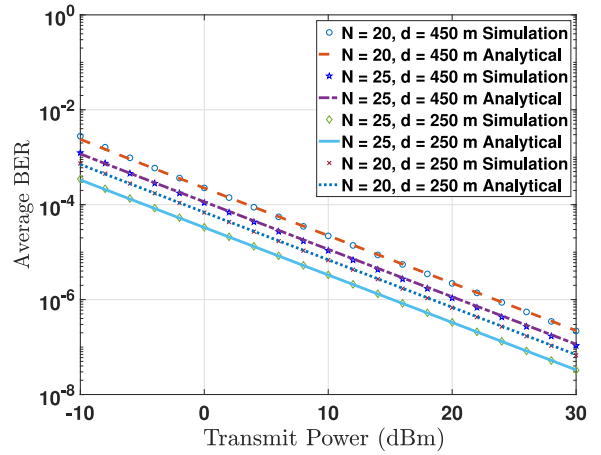

FIGURE 8. Average BER versus transmit power for varying d and N with $m = 1$, $k = 10$, $\Delta = 0.5$, $\sigma_\theta = 0.8°$, and $\sigma^2 = 1$.

respectively. It is important to observe that variations in m and Δ have a more pronounced impact on the OP than variations in K. This observation is substantiated by the wider range of variation in the OP graph observed when m and Δ are altered, while the variation in the OP graph remains relatively smaller for changes in K.

Fig. 8 depicts how both transmission distance and antenna array size affect the average BER. It is evident from Fig. 8 that to enhance the system performance, one can choose to either reduce the transmission distance or increase the size of the antenna array. Fig. 9 demonstrates the influence of the pointing error on the average BER. The average BER undergoes significant changes as the transceiver instability is varied from 0.8° to 1.2°. The impact of fading parameters m, K, and Δ (with $\sigma^2 = 1$) on the average BER is illustrated in Figs. 10, 11, and 12, respectively. Note that the average BER exhibits greater sensitivity to variations in m and Δ compared to changes in K. This observation is supported by the wider range of variation in the BER graph observed when m and Δ are altered, while the variation in the BER graph remains relatively smaller for changes in K.

Fig. 13 illustrates the impact of both transmission distance and antenna array size on the average channel capacity. In Fig. 13, it is noticeable that the system performance

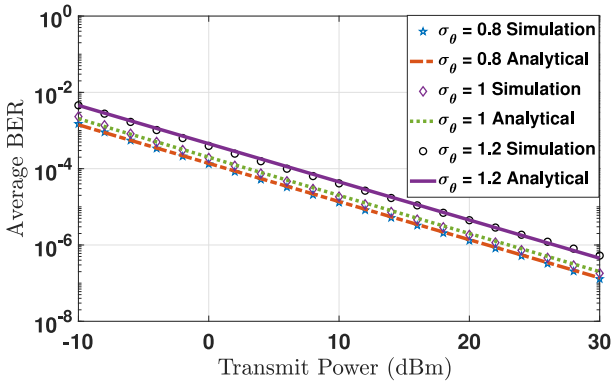

FIGURE 9. Average BER versus transmit power for varying σ_θ (in degrees) with parameters $d = 450$ m, $N = 25$, $m = 2.3$, $K = 10$, $\sigma^2 = 1$, and $\Delta = 0.9$.

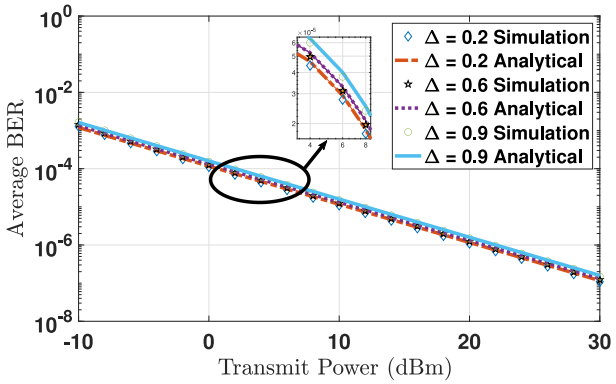

FIGURE 12. Average BER versus transmit power for varying Δ with $d = 450$ m, $N = 25$, $m = 1$, $K = 10$, $\sigma^2 = 1$, and $\sigma_\theta = 0.8°$.

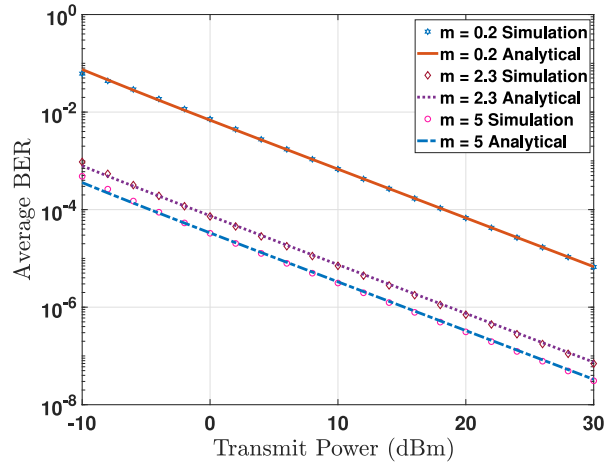

FIGURE 10. Average BER versus transmit power for varying m with $d = 450$ m, $N = 25$, $\sigma_\theta = 0.8°$, $K = 10$, $\sigma^2 = 1$, and $\Delta = 0.5$.

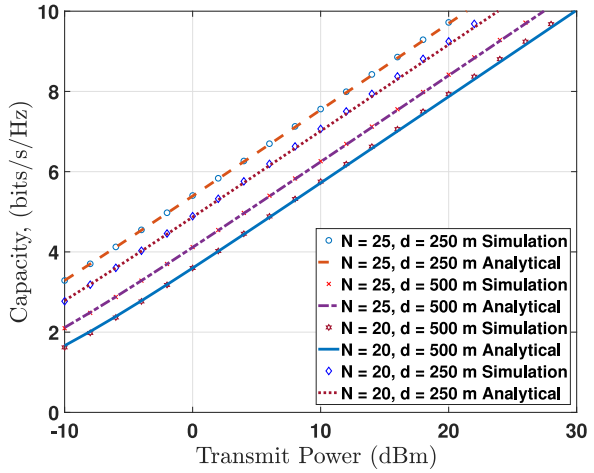

FIGURE 13. Capacity (referring to average channel capacity per unit bandwidth) versus transmit power for varying d and N with $\sigma_\theta = 1°$, $m = 1$, $K = 10$, $\sigma^2 = 1$, and $\Delta = 0.5$.

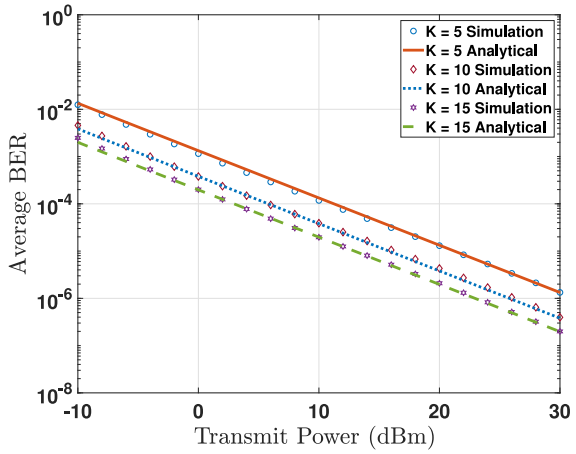

FIGURE 11. Average BER versus transmit power for varying K with $d = 450$ m, $N = 25$, $\sigma^2 = 1$, $\sigma_\theta = 0.8°$, $m = 1$, and $\Delta = 0.5$.

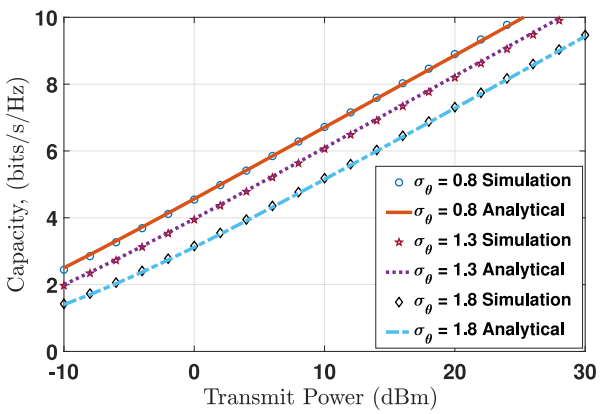

FIGURE 14. Capacity (referring to average channel capacity per unit bandwidth) versus transmit power for varying σ_θ (in degrees) with $d = 450$ m, $N = 25$, $m = 1$, $K = 10$, $\sigma^2 = 1$, and $\Delta = 0.5$.

experiences enhancement when the transmission distance is decreased while maintaining a constant antenna array size, or when the antenna array size is increased while keeping the transmission distance constant. The impact of transceiver instability on the average channel capacity is presented in Fig. 14. Subsequently, Figs. 15, 16, and 17 depict the impact of FTR fading parameters m, K, and Δ (with $\sigma^2 = 1$) on the average channel capacity, respectively.

Note that the average channel capacity displays greater sensitivity to variations in m and Δ compared to changes

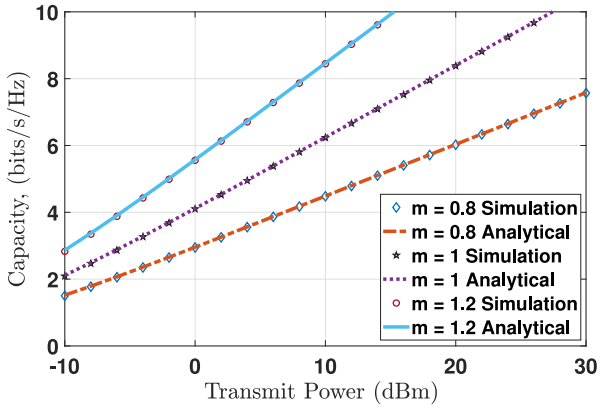

FIGURE 15. Capacity (referring to average channel capacity per unit bandwidth) versus transmit power for varying m with $d = 450$ m, $N = 25$, $\sigma_\theta = 1.2°$, $K = 10$, $\sigma^2 = 1$, and $\Delta = 0.5$.

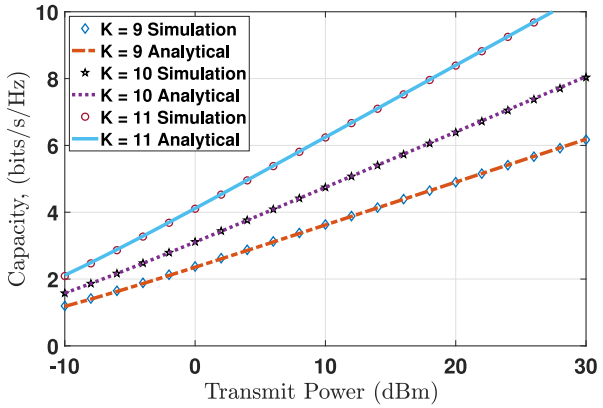

FIGURE 16. Capacity (referring to average channel capacity per unit bandwidth) versus transmit power for varying K with $d = 450$ m, $N = 25$, $\sigma^2 = 1$, $m = 1$, $\Delta = 0.5$, and $\sigma_\theta = 1.2°$.

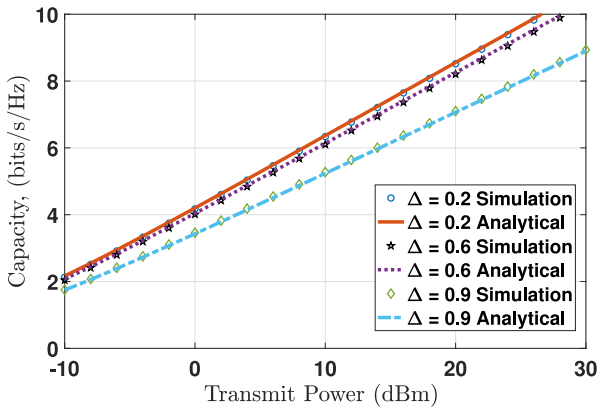

FIGURE 17. Capacity (referring to average channel capacity per unit bandwidth) versus transmit power for varying Δ with $d = 450$ m, $N = 25$, $m = 1$, $K = 10$, $\sigma^2 = 1$, and $\sigma_\theta = 1.2°$.

in K. This is evident from the significant variation observed in the channel capacity graph with even minor adjustments to m and Δ, whereas the variation in the channel capacity graph for modifications in K remains relatively smaller. The slight discrepancy between the simulation and analytical results of the OP and the average BER arises due to the neglecting of the effect of lower instantaneous SNR coefficients of the side lobes on the pointing error. However, since the capacity of the channel primarily relies on the behavior at high SNR, the impact of the side lobes on the capacity is negligible. As a result, the simulation and analytical results for the average channel capacity demonstrate an almost perfect match. Table 3 summarizes the effects of system and channel parameters on system performance.

TABLE 3. System performance with system/channel parameters.

Parameter	System Performance
N	Improves with increasing N
d	Degrades with increasing d
m	Improves with increasing m
K	Improves with increasing K
Δ	Degrades with increasing Δ
σ_θ	Degrades with increasing σ_θ

VI. CONCLUSION AND FUTURE DIRECTIONS

This study investigates the effects of the transmission distance, the size of the antenna array, the FTR fading parameters, and the pointing errors on the system performance for THz wireless transmission with fluctuating transmitter and receiver. Analytical closed-form expressions for the PDF, the CDF, and the MGF of the received instantaneous SNR are derived in terms of the single variate Fox's H function. Additionally, the nth moment of the instantaneous received SNR is computed. Furthermore, closed-form expressions for the OP, the average BER, and the average channel capacity are derived. To gain a more comprehensive understanding of the system under consideration, the diversity order of the system is computed. The validity of the derived closed-form expressions for the OP, the average BER, and the average channel capacity is confirmed as the simulation results closely match the analytical results. The numerical results provide evidence that the system performance shows improvement when either the transmission distance is reduced while maintaining a constant antenna array size, or when the antenna array size is increased while keeping the transmission distance constant. This improvement is observed in terms of the OP, the average BER, and the average channel capacity. Furthermore, Numerical results show that the system performance declines when σ_θ or Δ increases, whereas the system performance improves as the fading parameters m and K are increased. As the research progresses, it is important to consider hardware imperfections with pointing errors and fading. In addition to this, alternative fading distributions may be taken into account for the performance analysis of the system. These considerations will contribute to a more comprehensive understanding of the

practical implications and potential optimizations for THz wireless transmission.

APPENDIX A
PROOF OF THEOREM 1

From (8) and [36] we can easily write the PDF of h_p^2 as

$$f_{h_p^2}(y) = -\frac{\phi^2}{4} y^{\left(\frac{\phi}{2}-1\right)} \ln(y) \quad 0 < y < 1. \tag{27}$$

Assume that random variable $|h_i|^2 = |h_f|^2 h_p^2$. Using (8) and [38], the PDF of $|h_i|^2$ can be written as

$$f_{|h_i|^2}(x) = \int_0^1 \frac{1}{y} f_{|h_f|^2}\left(\frac{x}{y}\right) f_{h_p^2}(y)\, dy. \tag{28}$$

Substituting (5) and (27) in (28) and interchanging the summation and integration, (28) can be rewritten as

$$f_{|h_i|^2}(x) = \frac{-\phi^2 m^m}{4\Gamma(m)} \sum_{r=0}^{\infty} \frac{K^r d_r x^r}{(\Gamma(r+1))^2 (2\sigma^2)^{r+1}} \times \underbrace{\int_0^1 y^{\left(\frac{\phi}{2}-2-r\right)} \ln(y) \exp\left(-\frac{x}{2\sigma^2 y}\right) dy}_{I_2}. \tag{29}$$

We express the exponential in (29) in terms of the Meijer G-function [35, eq. (2.9.4) and eq. (2.9.1)] as

$$\exp\left(-\frac{x}{2\sigma^2 y}\right) = G_{0,1}^{1,0}\left[\frac{x}{2\sigma^2 y}\middle| \begin{matrix} - \\ 0 \end{matrix}\right]. \tag{30}$$

Now representing the Meijer G-function in terms of the multiple Barnes type integral [35, eq. (2.9.1)], we get

$$G_{0,1}^{1,0}\left[\frac{x}{2\sigma^2 y}\middle| \begin{matrix} - \\ 0 \end{matrix}\right] = \frac{1}{2\pi \jmath} \oint_{\mathcal{L}} \Gamma(s) \left(\frac{x}{2\sigma^2 y}\right)^{-s} ds \tag{31}$$

where $\mathcal{L}$ is the infinite contour defined in [35, eq. (1.1.6)]. Using (30), (31), and implementing a variable conversion, the inner integration I_2 of (29) can be rewritten as

$$I_2 = -\frac{1}{2\pi \jmath} \oint_{\mathcal{L}} \Gamma(s) \left(\frac{x}{2\sigma^2}\right)^{-s} \int_0^{\infty} t \times \exp\left(-t\left(\frac{\phi}{2} - 1 - r + s\right)\right) dt ds. \tag{32}$$

By using [36, eq. (3.381.4) and eq. (8.331.1)], the integration I_2 is further simplified as

$$I_2 = -\frac{1}{2\pi \jmath} \oint_{\mathcal{L}} \frac{\Gamma(s)\Gamma^2\left(\frac{\phi}{2} - r - 1 + s\right)}{\Gamma^2\left(\frac{\phi}{2} - r + s\right)} \left(\frac{x}{2\sigma^2}\right)^{-s} ds. \tag{33}$$

Using [35, eqs. (1.1.1) and (1.1.2)], I_2 is written in terms of the Fox's H-function as

$$I_2 = -H_{2,3}^{3,0}\left[\frac{x}{2\sigma^2}\middle| \begin{matrix} (a,1),(a,1) \\ (0,1),(a-1,1),(a-1,1) \end{matrix}\right]. \tag{34}$$

Substituting (34) in (29), the expression for the PDF of $|h_i|^2$ becomes

$$f_{|h_i|^2}(x) = \frac{\phi^2 m^m}{4\Gamma(m)} \sum_{r=0}^{\infty} \frac{K^r d_r x^r}{(\Gamma(r+1))^2 (2\sigma^2)^{r+1}} \times H_{2,3}^{3,0}\left[\frac{x}{2\sigma^2}\middle| \begin{matrix} (a,1),(a,1) \\ (0,1),(a-1,1),(a-1,1) \end{matrix}\right]. \tag{35}$$

The closed-form expression (9) for the PDF of γ is easily obtained from (35) by using

$$f_{\gamma}(z) = \frac{1}{\gamma_0 S_0^2 h_l^2} f_{|h_i|^2}\left(\frac{x}{\gamma_0 S_0^2 h_l^2}\right). \tag{36}$$

Evaluating $F_{\gamma}(z) = \int_0^z f_{\gamma}(x)\, dx$ by using (35) and (36), and repeating the same approaches used to obtain the PDF, the closed-form expression (10) for the CDF of γ is obtained.

The moment-generating function of instantaneous received SNR is by defining the integral [38, eq. (5.94)]

$$M_{\gamma}(\omega) = \int_0^{\infty} f_{\gamma}(z) e^{\jmath \omega z} dz. \tag{37}$$

We express the exponential term in (37) in terms of the Fox's H-function [35, eq. (2.9.4)] as

$$\exp(\jmath \omega z) = H_{0,1}^{1,0}\left[-\jmath \omega z\middle| \begin{matrix} - \\ (0,1) \end{matrix}\right]. \tag{38}$$

Substituting (38) and (9) in (37) and after changing the order of integration and summation, the expression of $M_{\gamma}(\omega)$ equals

$$M_{\gamma}(\omega) = \frac{\phi^2 m^m}{4\delta\Gamma(m)} \sum_{r=0}^{\infty} \frac{K^r d_r}{(2\sigma^2)^r \Gamma^2(r+1)\left(S_0^2 \gamma_0 h_l^2\right)^r} \times \int_0^{\infty} z^r H_{2,3}^{3,0}\left[\frac{z}{\delta}\middle| \begin{matrix} (a,1),(a,1) \\ (0,1),(a-1,1),(a-1,1) \end{matrix}\right] \times H_{0,1}^{1,0}\left[-\jmath \omega z\middle| \begin{matrix} - \\ (0,1) \end{matrix}\right] dz \tag{39}$$

Finally making the use of [35, eq. (2.8.4)] to solve the inner integration of (39), we readily obtain a closed-form expression for the moment-generating function as shown in (11). This completes the proof of Theorem 1.

APPENDIX B
PROOF OF LEMMA 1

The nth moment of the instantaneous received SNR is defined as

$$\bar{\gamma}^{(n)} \triangleq \int_0^{\infty} z^n f_{\gamma}(z) dz. \tag{40}$$

Using (9) in (40) and after changing the order of integration and summation, the nth moment of the instantaneous received SNR is given as

$$\bar{\gamma}^{(n)} = \frac{\phi^2 m^m}{4\delta\Gamma(m)} \sum_{r=0}^{\infty} \frac{K^r d_r}{(2\sigma^2)^r \Gamma^2(r+1)\left(S_0^2 \gamma_0 h_l^2\right)^r} \times \int_0^{\infty} z^n z^r H_{2,3}^{3,0}\left[\frac{z}{\delta}\middle| \begin{matrix} (a,1),(a,1) \\ (0,1),(a-1,1),(a-1,1) \end{matrix}\right] dz \tag{41}$$

We express the polynomial term z^r in (41) in terms of Fox's H-function as [35, eq. (2.9.6)]

$$z^r = H_{1,1}^{1,0}\left[z\middle| \begin{matrix} (r+1,1) \\ (r,1) \end{matrix}\right]. \tag{42}$$

Inserting (42) in (41) and making the use of identity [35, eq. (2.8.4)] to solve the inner integration, the nth moment of the instantaneous received SNR is obtained as (12). This completes the proof of Lemma 2.

APPENDIX C
PROOF OF THEOREM 2

The ergodic mutual information for M-QAM constellation is obtained as

$$\bar{C_m} = \int_0^\infty I(\gamma) f_\gamma(\gamma) d\gamma, \tag{43}$$

where $I(\gamma)$ represents the instantaneous mutual information, and for the $M-QAM$ constellation, it can be estimated as [39]

$$I(\gamma) \simeq \log_2(M)\left(1 - \sum_{\tau=0}^{k_M} \epsilon_\tau e^{-V_\tau \gamma}\right). \tag{44}$$

The coefficients k_M, ϵ_τ, and V_τ are given for different values of M in [39, Table I]. Inserting (9) and (44) into (43), we obtain

$$\bar{C}(\gamma) \simeq \log_2(M)\left(1 - \sum_{\tau=0}^{k_M} \epsilon_\tau I_{3\tau}\right), \tag{45}$$

where

$$\begin{aligned} I_{3\tau} = &\int_0^\infty z^r e^{-V_\tau z} \frac{\phi^2 m^m}{4\delta\Gamma(m)} \\ &\times \sum_{r=0}^{\infty} \frac{K^r d_r}{\left(2\sigma^2\right)^r \Gamma^2(r+1)\left(S_0^2\gamma_0 h_l^2\right)^r} \\ &\times H_{2,3}^{3,0}\left[\frac{z}{\delta}\middle| \begin{matrix}(a,1),(a,1)\\(0,1),(a-1,1),(a-1,1)\end{matrix}\right] dz. \end{aligned} \tag{46}$$

Expressing the exponential term in (46) in terms of the Fox's H-function and after changing the order of integration and summation we get

$$\begin{aligned} I_{3\tau} = &\frac{\phi^2 m^m}{4\delta\Gamma(m)} \sum_{r=0}^{\infty} \frac{K^r d_r}{\left(2\sigma^2\right)^r \Gamma^2(r+1)\left(S_0^2\gamma_0 h_l^2\right)^r} \\ &\times \int_0^\infty z^r H_{2,3}^{3,0}\left[\frac{z}{\delta}\middle| \begin{matrix}(a,1),(a,1)\\(0,1),(a-1,1),(a-1,1)\end{matrix}\right] \\ &\times H_{0,1}^{1,0}\left[V_\tau z\middle| \begin{matrix}-\\(0,1)\end{matrix}\right] dz. \end{aligned} \tag{47}$$

Subsequently, by applying [35, eq. (2.8.4)] to solve the inner integration of $I_{3\tau}$, and substituting the resulting value of $I_{3\tau}$ into (45), we efficiently arrive at a closed-form representation for the ergodic mutual information as presented in (24). This finalizes the verification of Theorem 2.

REFERENCES

[1] T. S. Rappaport et al., "Wireless communications and applications above 100 GHz: Opportunities and challenges for 6G and beyond," *IEEE Access*, vol. 7, pp. 78729–78757, 2019.

[2] I. F. Akyildiz, A. Kak, and S. Nie, "6G and beyond: The future of wireless communications systems," *IEEE Access*, vol. 8, pp. 133995–134030, 2020.

[3] Q. Tang, F. R. Yu, R. Xie, A. Boukerche, T. Huang, and Y. Liu, "Internet of intelligence: A survey on the enabling technologies, applications, and challenges," *IEEE Commun. Surveys Tuts.*, vol. 24, no. 3, pp. 1394–1434, 3rd Quart., 2022.

[4] W. Jiang, B. Han, M. A. Habibi, and H. D. Schotten, "The road towards 6G: A comprehensive survey," *IEEE Open J. Commun. Soc.*, vol. 2, pp. 334–366, 2021.

[5] X. Yu et al., "Exploring THz band for high speed wireless communications," in *Proc. 41st Int. Conf. Infrared Millimeter THz Waves (IRMMW-THz)*, Copenhagen, Denmark, Sep. 2016, pp. 1–2.

[6] H. Elayan, O. Amin, B. Shihada, R. M. Shubair, and M.-S. Alouini, "Terahertz band: The last piece of RF spectrum puzzle for communication systems," *IEEE Open J. Commun. Soc.*, vol. 1, pp. 1–32, 2020.

[7] Z. Chen et al., "A survey on terahertz communications," *China Commun.*, vol. 16, no. 2, pp. 1–35, Feb. 2019.

[8] K. Zhi et al., "Two-timescale design for reconfigurable intelligent surface-aided massive MIMO system with imperfect CSI," *IEEE Trans. Inf. Theory*, vol. 69, no. 5, pp. 3001–3033, May 2023.

[9] K. Zhi, C. Pan, H. Ren, and K. Wang, "Power scaling law analysis and phase shift optimization of RIS-aided massive MIMO systems with statistical CSI," *IEEE Trans. Commun.*, vol. 70, no. 5, pp. 3558–3574, May 2022.

[10] R. K. Mallik, "A new statistical model of the complex Nakagami-m fading gain," *IEEE Trans. Commun.*, vol. 58, no. 9, pp. 2611–2620, Sep. 2010.

[11] G. D. Durgin, T. S. Rappaport, and D. A. D. Wolf, "New analytical models and probability density functions for fading in wireless communications," *IEEE Trans. Commun.*, vol. 50, no. 6, pp. 1005–1015, Jun. 2002.

[12] J. M. Romero-Jerez, F. J. Lopez-Martinez, J. F. Paris, and A. J. Goldsmith, "The fluctuating two-ray fading model: Statistical characterization and performance analysis," *IEEE Trans. Wireless Commun.*, vol. 16, no. 7, pp. 4420–4432, Jul. 2017.

[13] M. K. Samimi, G. R. MacCartney, S. Sun, and T. S. Rappaport, "28 GHz millimeter-wave ultrawideband small-scale fading models in wireless channels," in *Proc. IEEE 83rd Veh. Technol. Conf. (VTC Spring)*, May 2016, pp. 1–6.

[14] H. Du, J. Zhang, K. Guan, B. Ai, and T. Karner, "Reconfigurable intelligent surface aided terahertz communications under misalignment and hardware impairments," 2020, *arXiv:2012.00267*.

[15] A.-A. A. Boulogeorgos, E. N. Papasotiriou, and A. Alexiou, "Analytical performance assessment of THz wireless systems," *IEEE Access*, vol. 7, pp. 11436–11453, 2019.

[16] A. A. Joshi, P. Bhardwaj, and S. M. Zafaruddin, "Terahertz wireless transmissions with maximal ratio combining over fluctuating two-ray fading," in *Proc. IEEE Wireless Commun. Netw. Conf. (WCNC)*, Austin, TX, USA, 2022, pp. 1575–1580.

[17] M. T. Dabiri and M. Hasns, "Pointing error modeling of mmWave to THz high-directional antenna arrays," *IEEE Wireless Commun. Lett.*, vol. 11, no. 11, pp. 2435–2439, Nov. 2022.

[18] O. S. Badarneh, M. T. Dabiri, and M. Hasns, "Channel modeling and performance analysis of directional THz links under pointing errors and $\alpha-\mu$ distribution," *IEEE Wireless Commun. Lett.*, vol. 27, no. 3, pp. 812–816, Mar. 2023.

[19] H. Zhao, Z. Liu, and M.-S. Alouini, "Different power adaption methods on fluctuating two-ray fading channels," *IEEE Wireless Commun. Lett.*, vol. 8, no. 2, pp. 592–595, Apr. 2019.

[20] W. Zeng, J. Zhang, S. Chen, K. P. Peppas, and B. Ai, "Physical layer security over fluctuating two-ray fading channels," *IEEE Trans. Veh. Technol.*, vol. 67, no. 9, pp. 8949–8953, Sep. 2018.

[21] Y. Zhang, J. Zhang, L. Yang, B. Ai, and M.-S. Alouini, "On the performance of dual-hop systems over mixed FSO/mmWave fading channels," *IEEE Open J. Commun. Soc.*, vol. 1, pp. 477–489, 2020.

[22] O. S. Badarneh and D. B. da Costa, "Cascaded fluctuating two-ray fading channels," *IEEE Commun. Lett.*, vol. 23, no. 9, pp. 1497–1500, Sep. 2019.

[23] H. Du et al., "Performance and optimization of reconfigurable intelligent surface aided THz communications," *IEEE Trans. Commun.*, vol. 70, no. 5, pp. 3575–3593, May 2022.

[24] A. A. Farid and S. Hranilovic, "Outage capacity optimization for free-space optical links with pointing errors," *J. Lightw. Technol.*, vol. 25, no. 7, pp. 1702–1710, Jul. 2007.

[25] O. S. Badarneh, "Performance analysis of terahertz communications in random fog conditions with misalignment," *IEEE Wireless Commun. Lett.*, vol. 11, no. 5, pp. 962–966, May 2022.
[26] P. Bhardwaj and S. M. Zafaruddin, "Performance of dual-hop relaying for THz-RF wireless link over asymmetrical α-μ fading," *IEEE Trans. Veh. Technol.*, vol. 70, no. 10, pp. 10031–10047, Oct. 2021.
[27] A.-A. A. Boulogeorgos and A. Alexiou, "Outage probability analysis of THz relaying systems," in *Proc. IEEE 31st Annu. Int. Symp. Pers. Indoor Mobile Radio Commun.*, 2020, pp. 1–7.
[28] X. Tong, B. Chang, Z. Meng, G. Zhao, and Z. Chen, "Calculating terahertz channel capacity under beam misalignment and user mobility," *IEEE Wireless Commun. Lett.*, vol. 11, no. 2, pp. 348–351, Feb. 2022.
[29] A.-A. A. Boulogeorgos, J. M. Riera, and A. Alexiou, "On the joint effect of rain and beam misalignment in terahertz wireless systems," *IEEE Access*, vol. 10, pp. 58997–59012, 2022.
[30] M. T. Dabiri, M. Hasna, N. Zobra, T. Khattab, and K. A. Qaraqe, "A general model for pointing error of high frequency directional antennas," *IEEE Open J. Commun. Soc.*, vol. 3, pp. 1978–1990, 2022.
[31] J. Kokkoniemi, A.-A. A. Boulogeorgos, M. Aminu, J. Lehtomäki, A. Alexiou, and M. Juntti, "Impact of beam misalignment on THz wireless systems," *Nano Commun. Netw.*, vol. 24, May 2020, Art. no. 100302.
[32] J. Kokkoniemi, J. Lehtomaki, and M. Juntti, "Simplified molecular absorption loss model for 275–400 Gigahertz frequency band," in *Proc. 12th Eur. Conf. Ant. Propag. (EuCAP)*, London, U.K., Apr. 2018, pp. 1–5.
[33] J. Zhang, W. Zeng, X. Li, Q. Sun, and K. P. Peppas, "New results on the fluctuating two-ray model with arbitrary fading parameters and its applications," *IEEE Trans. Veh. Technol.*, vol. 67, no. 3, pp. 2766–2770, Mar. 2018.
[34] C. A. Balanis, *Antenna Theory: Analysis and Design*. Hoboken, NJ, USA: Wiley, 2016.
[35] A. A. Kilbas, *H-Transforms: Theory and Applications*. Boca Rotan, FL, USA: CRC Press, 2004.
[36] I. S. Gradshtyn and I. M. Ryzhik, *Table of Integrals, Series and Products*, 7th ed. New York, NY, USA: Academic, 2007.
[37] H. M. Srivastava and H. L. Manocha, *A Treatise on Generating Functions*. New York, NY, USA: Wiley, 1984.
[38] A. Papoulis and S. U. Pillai, *Probability, Random Variables, and Stochastic Processes.*, New York, NY, USA: McGraw-Hill Educ., 2002.
[39] C. Ouyang, S. Wu, C. Jiang, J. Cheng, and H. Yang, "Approximating ergodic mutual information for mixture gamma fading channels with discrete inputs," *IEEE Commun. Lett.*, vol. 24, no. 4, pp. 734–738, Apr. 2020.

ANIL YADAV (Graduate Student Member, IEEE) received the B.Tech. degree in electronics and communication engineering from Dr. A. P. J. Abdul Kalam Technical University, Lucknow, India, in 2019, and the M.Tech. degree from the Indian Institute of Technology Delhi, New Delhi, India, in 2021, where he is currently pursuing the Ph.D. degree with the Department of Electrical Engineering. His research interests include channel modeling, THz wireless communications, and cooperative communications.

RANJAN K. MALLIK (Fellow, IEEE) received the B.Tech. degree in electrical engineering from the Indian Institute of Technology Kanpur, Kanpur, in 1987, and the M.S. and Ph.D. degrees in electrical engineering from the University of Southern California, Los Angeles, in 1988 and 1992, respectively.

From August 1992 to November 1994, he was a Scientist with the Defence Electronics Research Laboratory, Hyderabad, India, working on missile and EW projects. From November 1994 to January 1996, he was a faculty member with the Department of Electronics and Electrical Communication Engineering, Indian Institute of Technology Kharagpur, Kharagpur. From January 1996 to December 1998, he was with the faculty of the Department of Electronics and Communication Engineering, Indian Institute of Technology Guwahati, Guwahati. Since December 1998, he has been with the faculty of the Department of Electrical Engineering, Indian Institute of Technology Delhi, New Delhi, where he is currently a Professor. His research interests are in diversity combining and channel modeling for wireless communications, space-time systems, cooperative communications, multiple-access systems, power line communications, molecular communications, difference equations, and linear algebra. He is a recipient of the Hari Om Ashram Prerit Dr. Vikram Sarabhai Research Award in the field of electronics, telematics, informatics, and automation, the Shanti Swarup Bhatnagar Prize in Engineering Sciences, the Khosla National Award, the IEI-IEEE Award for Engineering Excellence, and the J. C. Bose Fellowship. He has served as an Area Editor and an Editor for the IEEE TRANSACTIONS ON WIRELESS COMMUNICATIONS, and as an Editor for the IEEE TRANSACTIONS ON COMMUNICATIONS. He is a member of Eta Kappa Nu, the IEEE Communications, Information Theory, and Vehicular Technology Societies, the American Mathematical Society, the International Linear Algebra Society, and the Association for Computing Machinery; a Fellow of the Indian National Academy of Engineering, the Indian National Science Academy, The National Academy of Sciences, India, Prayagraj, the Indian Academy of Sciences, Bengaluru, The World Academy of Sciences-for the advancement of science in developing countries, The Institution of Engineering and Technology, U.K., The Institution of Electronics and Telecommunication Engineers, India, The Institution of Engineers (India), and the Asia–Pacific Artificial Intelligence Association; and a Life Member of the Indian Society for Technical Education.